Biophysical Journal, Volume 99

Supporting Material

A consistent picture of the reversible thermal unfolding of hen egg-white lysozyme (HEWL) from experiment and molecular dynamics

Filip Meersman, Canan Atilgan, Andrew J. Miles, Reto Bader, Weifeng Shang, André Matagne, B. A. Wallace, and Michel H.J. Koch

A consistent picture of the reversible thermal unfolding of hen egg-white lysozyme from experiment and molecular dynamics

Filip Meersman, Canan Atilgan, Andrew J. Miles, Reto Bader, Weifeng Shang, André Matagne, B.A. Wallace, Michel H.J. Koch

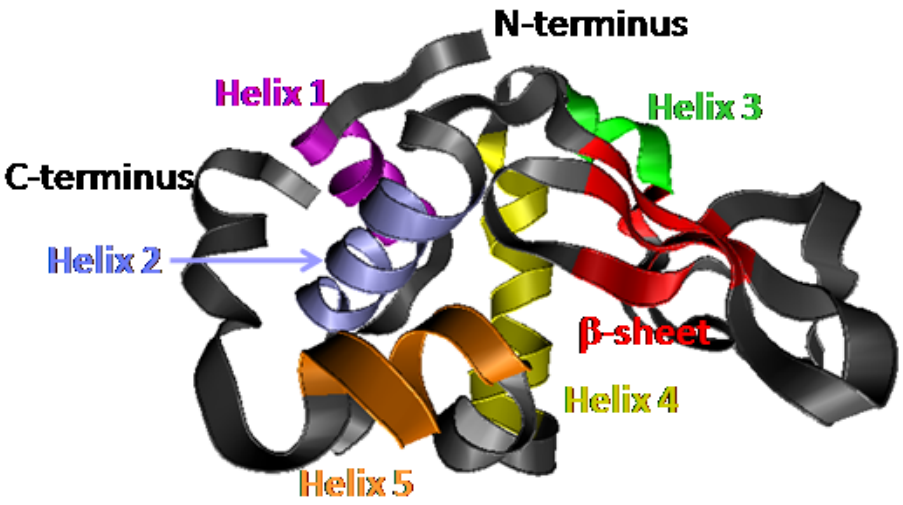

FIGURE S1: Initial model of HEWL for the MD simulations obtained after equilibrating the crystallographic model in PDB entry 6LYZ (1) for 2ns at 27°C. The color coding used here is the same as in Fig. 7. The first domain formed by helices 1, aa [5-15] (purple), 2 aa[25-36] (blue), 4 aa[88-101] (yellow), 5 aa[109-115] (orange) and the 3_{10} helix aa[120-124] is usually referred to as α-domain. The second domain (β-domain) (aa [37-84]) consists of sheet structures, aa[43-45], [51-53], [58-59], [64-65] and [78-79] (red) and of 3_{10} helix 3, aa[80,84] (green). Helices 1 to 4 are often referred to as A,B,C,D in the literature.

Materials and Methods

Synchrotron Radiation Circular Dichroism (SRCD) Spectroscopy

Far ultraviolet and vacuum ultraviolet SRCD spectra were measured on the CD1 beamline at the ASTRID facility of the ISA (Aarhus, DK). The instrument was calibrated using camphorsulfonic acid following each beam injection as described previously (2). The actual sample temperature (as opposed to the set temperature) was measured using a thermistor probe inserted in the sample cell. HEWL (Worthington Biochemical Corp., Lakewood, NJ) was dissolved in double distilled water at a concentration of 1 mg mL^{-1} (pH 5.9 at 20°C) in a 0.1 mm pathlength sealed cylindrical quartz Suprasil cell (Hellma, Müllheim,GE). The temperature was increased from set temperatures of 20°C to 80°C or from 20°C to 85°C in 5°C steps, allowing 3 minute equilibration at each temperature. The actual maximum temperatures were 70°C and 77°C, respectively. Three scans over the wavelength range from 280 to 175 nm, with a wavelength interval of 1 nm and a 2 s dwell time, were acquired at each temperature and the first and third scans were compared to ensure that the sample had reached

equilibrium before the measurements were made. Following the final temperature point the sample was allowed to cool to 20°C and equilibrated for 12 hours before re-measuring its spectrum. Data were processed using the CDTools software (3). The average of the three scans at each temperature was smoothed with a Savitsky-Golay filter before subtracting an averaged water baseline spectrum collected in the same sample cell.
Near UV CD spectra were measured between 340 nm and 240 nm, using a 0.5 nm step size and 2s averaging time, on an Aviv 62DS (AVIV Biomedical, Lakewood, NJ) spectropolarimeter in a 1 cm quartz Suprasil cell (Hellma, Müllheim, GE). The actual temperatures in this cell were calibrated against the set temperature. Data was collected from 20°C to the maximum temperature (80°C for the reversible experiment and 85°C for the irreversible) and again after the sample temperature had been returned to 20°C. For each temperature three scans were averaged and the average of three baseline scans of water in the same cell was subtracted.
Secondary structure analyses using the CONTINLL (4, 5) and CDDSTR (6, 7) algorithms were carried out on the SRCD data with the DichroWeb analysis server (8, 9). All SELCON3 analyses (10, 11) used the Matlab (The Mathworks, Natick, Mass) version of the algorithm, SELMAT (11). All analyses used the SP175 reference dataset (12). The results from the individual algorithms were averaged and the standard deviations between the calculated secondary structures are reported in Table 1. The goodness-of-fit parameter (NRMSD) values (13) are reported for the CONTINLL analyses, as these are the most sensitive to variations in structure. NRMSD values below 0.1 indicate a good correspondence between the calculated secondary structure and the experimental CD data. Singular value decomposition (SVD) analyses were carried out using the CDTool software (3).

FTIR spectroscopy HEWL (Sigma Aldrich, Munich) was dissolved in D_2O at a concentration of 50 mg mL^{-1}. Prior to the experiment the protein solution was heated to 80°C for 15 min to ensure full H/D-exchange.
Infrared spectra were recorded on a Bruker IFS66 FTIR spectrometer equipped with a liquid nitrogen cooled MCT detector at a nominal resolution of 2 cm^{-1}. Each spectrum is the result of the accumulation and averaging of 256 interferograms. The sample compartment was continuously purged with dry air to minimise the spectral contribution of atmospheric water.
Thermal unfolding was followed using a temperature cell with CaF_2 windows separated by a 50 μm teflon spacer. The cell was placed in a heating jacket controlled by a Graseby Specac (Orpington, UK) automatic temperature controller. Temperature scans were made at a rate of 0.5°C min^{-1}.
In order to enhance the component peaks contributing to the amide I' band, the spectra were treated by Fourier self-deconvolution using the Bruker software (OS/2 version). The lineshape was assumed to be Lorentzian with a half-bandwidth of 21 cm^{-1} and an enhancement factor *k* of 1.7 was used (14). A linear baseline correction was made in the amide I' region (1600-1700 cm^{-1}).

NMR Spectroscopy
Data were recorded on a HEWL solution (74 mg mL^{-1}, pH 3.8) in 90% H_2O and 10% D_2O with 1mM 4,4-dimethyl-4-silapentane-1-sulfonic acid (DSS) as calibration standard at a magnetic field strength of 11.75 T with a Bruker AVANCE 500 spectrometer equipped with a TXI probe operating at a ^1H resonance frequency of 500.13 MHz. NMR spectra were acquired at different temperatures between 35°C and 80°C. The temperature was calibrated by monitoring the chemical-shift separation between the OH resonances and CH_2 resonances of ethylene glycol in d_6-DMSO between 27°C and 107°C.
^1H chemical shifts were referenced to DSS used as internal standard. ^{15}N chemical shifts were indirectly referenced to DSS following standard procedures (15). ^1H-^{15}N -HSQC experiments

on a protein sample with natural ^{15}N abundance were recorded with 128 x 2048 complex data points using a sweep width of 11160 Hz in the ^{1}H dimension and 2000 Hz in the ^{15}N dimension. 2D homonuclear correlations via dipolar coupling were measured using a NOESY experiment with phase sensitive water suppression (16). For NOESY spectra a mixing time of 120 ms was used. All spectra were processed and analyzed using the TOPSPIN 2.1 software (Bruker Biospin) and AUREMOL (17)

Small angle X-ray scattering

HEWL was dissolved and extensively dialysed against distilled Na-acetate buffer (pH 3.8) at concentrations between 3 and 50 mg mL^{-1}. X-ray scattering patterns of solutions and buffers were recorded in the range ($3\ 10^{-2}$ $Å^{-1} \leq Q \leq 0.6$ $Å^{-1}$ ($Q = 4\pi\sin\theta/\lambda$, 2θ is the scattering angle and λ =1.5 Å, the X-ray wavelength) on the X33 beamline (18) of the EMBL on the storage ring DORIS at the Deutsches Elektronen Synchrotron (DESY) in Hamburg following standard procedures (19) using gas proportional detectors (20). Samples with concentrations between 5 and 50 mg mL^{-1} were placed in a 1 mm pathlength thermostated cell with mica windows. The data were analyzed using the OTOKO (21), GNOM (22) and GASBOR (23) programs.

Molecular Dynamics simulations

All calculations to model the dynamics of the HEWL – water system were carried out with the NAMD software (24). A single HEWL (protein data bank (25) (PDB) code 6LYZ (1)) molecule was soaked in a solvent box containing 2271 TIP3P water molecules and eight chloride ions were added for charge neutrality. The resulting system with an cubic periodic cell of $(54\ Å)^3$ used as initial structure, consisted of a total of 10281 atoms, prepared using the VMD 1.8.6 program with solvate plug-in version 1.2 (26). The CharmM27 force field parameters were used (27) and electrostatic interactions were calculated via a partial mesh Ewald method (28). The cutoff distance for non-bonded van der Waals interactions was set to 12 Å with a switching function cutoff of 10 Å. The bond lengths were fixed to their average values using the RATTLE algorithm (29). Prior to the simulations the energy of the system was first minimized using the conjugate gradients method until the gradient tolerance was below 10^{-2} kcal/mol/Å. MD simulations in the NVT ensemble at 57°C and 67°C, corresponding to the region where the calculated heat capacity (C_p) starts increasing in the simulations of C_p vs T (data not shown), were carried out for 2 ns, followed by 8 and 10 ns runs for the respective temperatures in the NPT ensemble. Nine structures were selected from the two simulations at the 2, 4, 6, 8 and 10 ns time points, subjected to minimization followed by 10 ns long NPT simulations at 227°C and 1 atm. Volumetric fluctuations were preset to be isotropic. The temperature was controlled by Langevin dynamics with a damping coefficient of 5/ps and the pressure by a Langevin piston. The Verlet algorithm was used in all runs for integrating the equations of motion with a time-step of 2 fs (30). All MD results discussed in the paper are based on these nine trajectories, which are labeled run1 to run9.

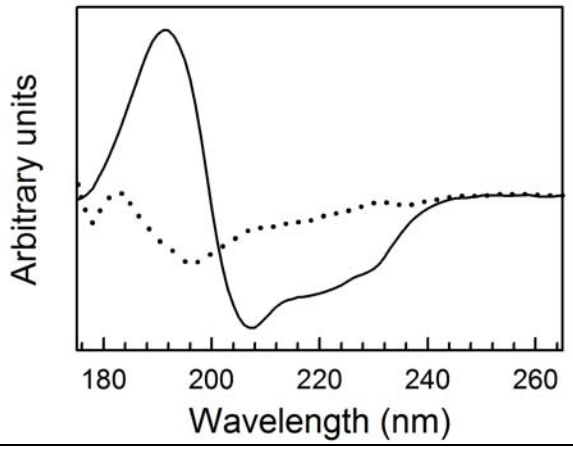

FIGURE S2A: Component curves (arbitrary units) derived from the SVD analysis of the SRCD data. The first component (solid line) is representative of a folded protein. The second component (dotted line), which has been multiplied by 5, represents the spectrum of a disordered polypeptide.

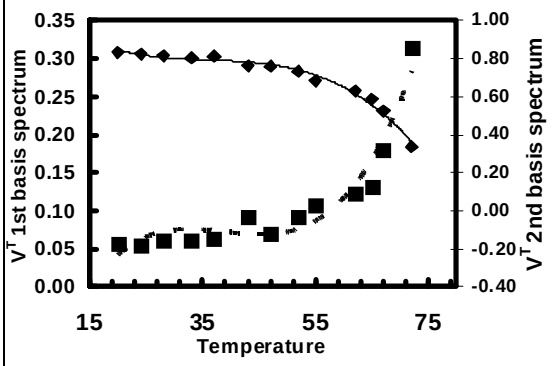

FIGURE S2B: Components present at each temperature from the SVD analysis of the SRCD data: The two row vectors in the V^T matrix corresponding to the first (♦) and second (■) most important component CD spectra, indicating the relative proportion of each component present.

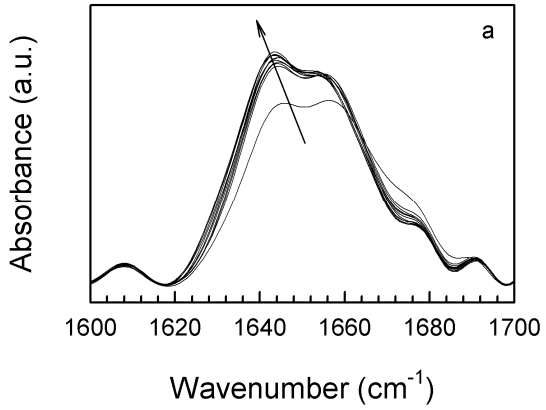

FIGURE S3A: Temperature-induced changes in the IR spectrum (amide I band region) of HEWL between 20°C and 80°C. The arrow indicates the direction of the spectral changes during cooling.

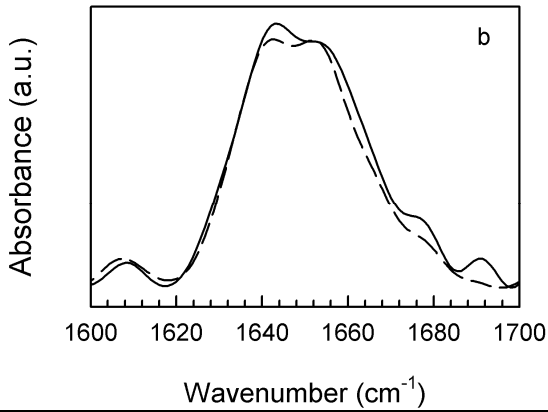

FIGURE S3B: Comparison of the spectra at 25°C before (solid line) and after (dashed line) thermal unfolding.

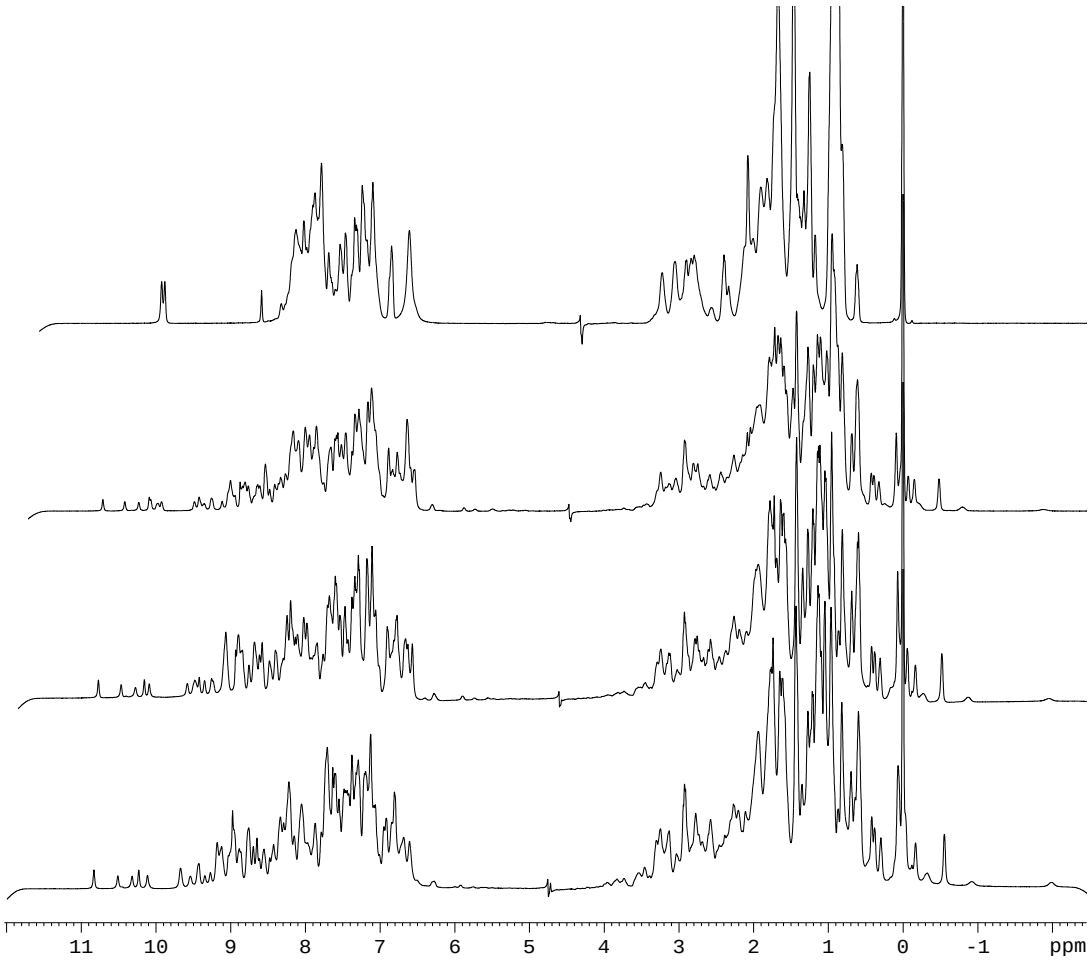

FIGURE S4: Thermal denaturation (T_M=74°C) of HEWL (5mM, pH 3.8) monitored by 1D ^{1}H NMR; from bottom to top: 37°C, 52°C, 66°C and 80°C.

Table S1: Amide proton chemical shifts of HEWL at 37°C (31)and 70°C and their difference (Δ), configuration of the residues in the NMR structure in PDB entry 193l (32), according to the STRIDE algorithm (33) (B: isolated β-bridge, C: coil, E: extended configuration (β-sheet), G: 3_{10} helix) H: α-helix, T: turn). Differences in the residue configurations in the crystallographic model in PDB entry 1E8L (32) are indicated in red. The asterisks mark where the average of the differences between the chemical shifts of the amide protons (Δ^1H^N) at 37°C and 70°C in three successive residues is above -0.07 ppm and the structure is unfolded. The crosses indicated residues which are additionally marked if one requires the average of the absolute values of the differences for three successive residue to be above 0.07 ppm. The last three columns are the ^{15}N chemical shifts at 37°C (34) and 70°C and their difference ($\Delta^{15}N$).
The cells marked in yellow are those for which amide hydrogen exchange protection factors were determined at 69°C (35).

	Amide proton chemical shifts			Config.	^{15}N chemical shifts		
Residue	37°C	70°C	Δ^1H^N		37°C	70°C	$\Delta^{15}N$
THR 1				C			
VAL 2	8.96	8.814	-0.146	B	127.72	127.732	-0.012
PHE 3	8.87	8.803	-0.067	C+	127.80	128.224	-0.424
GLY 4	8.51	8.514	0.004	C	104.86	105.019	-0.159
ARG 5	8.56	8.498	-0.062	H	122.92	122.775	0.145
CYS 6	8.60	8.509	-0.091	H*	114.84	114.793	0.047
GLU 7	8.14	7.991	-0.149	H*	125.30	125.025	0.275
LEU 8	8.63	8.536	-0.094	H*	120.56	120.419	0.141
ALA 9	8.40	8.324	-0.076	H	121.56	121.509	0.051
ALA 10	8.17	8.149	-0.021	H	118.40	118.626	-0.226
ALA 11	7.79	7.830	0.040	H	121.56	121.438	0.122
MET 12	9.10	8.983	-0.117	H	118.66	118.379	0.281
LYS 13	8.54	8.531	-0.009	H	122.06	122.212	-0.152
ARG 14	8.25	8.177	-0.073	H	120.14	120.138	0.002
HIS 15	7.32	7.327	0.007	H	112.48	113.035	-0.555
GLY 16	7.62	7.675	0.055	C	106.14	106.425	-0.285
LEU 17	7.15	7.196	0.046	T+	115.24	115.672	-0.432
ASP 18	8.71	8.531	-0.179	T*	117.92	117.782	0.138
ASN 19	8.35	8.265	-0.085	T*	123.18	122.950	0.230
TYR 20	8.08	8.035	-0.045	GT*	125.30	124.919	0.381
ARG 21	8.93	8.803	-0.127	GT	126.10	126.150	-0.050
GLY 22	7.60	7.599	-0.001	GT	101.88	101.924	-0.044
TYR 23	7.66	7.686	0.026	CT	119.20	119.434	-0.234
SER 24	8.98	8.934	-0.046	C+	121.96	122.117	-0.157
LEU 25	9.09	8.917	-0.173	H*	121.68	122.001	-0.321
GLY 26	9.59	9.468	-0.122	H*	105.02	104.808	0.212
ASN 27	8.19	8.182	-0.008	H	117.00	117.325	-0.325

TRP 28	7.19	7.245	0.055	H	120.26	120.208	0.052
VAL 29	7.57	7.572	0.002	H	118.78	118.731	0.049
CYS 30	8.01	7.980	-0.030	H	118.42	118.344	0.076
ALA 31	8.12	8.066	-0.054	H	119.06	118.766	0.294
ALA 32	7.60	7.626	0.026	H	117.18	117.254	-0.074
LYS 33	7.95	7.937	-0.013	H	119.82	119.927	-0.107
PHE 34	7.34	7.327	-0.013	H	114.28	114.969	-0.689
GLU 35	8.58	8.520	-0.060	H	116.98	117.043	-0.063
SER 36	7.94	7.915	-0.025	H	108.64	108.746	-0.106
ASN 37	8.14	8.193	0.053	T	125.66	125.271	0.389
PHE 38	7.35	7.414	0.064	T	105.04	105.194	-0.154
ASN 39	7.41	7.452	0.042	B+	117.72	117.993	-0.273
THR 40	9.38	9.261	-0.119	T+	115.18	115.391	-0.211
GLN 41	7.90	7.879	-0.050	T			-0.100
ALA 42	6.86	6.880	0.020	T	122.34	122.388	-0.048
THR 43	8.27	8.171	-0.099	E	114.84	114.758	0.082
ASN 44	8.15	8.106	-0.044	E*	119.80	120.173	-0.373
ARG 45	8.85	8.656	-0.194	E*	126.20	126.396	-0.196
ASN 46	8.89	8.77	-0.120	T*	121.68	121.685	-0.005
THR 47	8.80	8.683	-0.117	T*	114.10	114.020	0.080
ASP 48	7.81	7.792	-0.018	T	118.22	118.379	-0.159
GLY 49	7.88	7.877	-0.003	T	107.80	107.831	-0.031
SER 50	8.25	8.231	-0.019	C	116.14	116.200	-0.060
THR 51	9.12	9.032	-0.088	E	117.60	117.887	-0.287
ASP 52	8.80	8.825	0.025	E	124.22	125.060	-0.840
TYR 53	9.02	8.977	-0.043	E	118.58	118.379	0.201
GLY 54	9.04	9.010	-0.030	T*	111.60	111.558	0.042
ILE 55	9.27	9.086	-0.184	T*	121.02	120.911	0.109
LEU 56	8.89	8.819	-0.071	T*	119.04	119.188	-0.148
GLN 57	7.95	7.844	-0.106	T	114.70	114.828	-0.128
ILE 58	7.68	7.713	0.033	E C*	121.10	121.333	-0.233
ASN 59	8.52	8.351	-0.169	E T+	127.22	126.396	0.824
SER 60	9.18	9.233	0.053	T+	119.56	120.278	-0.718
ARG 61	8.78	8.764	-0.016	T	123.26	123.196	0.064
TRP 62	7.19	7.338		T	114.46	113.633	0.827
TRP 63	7.43	7.332	-0.098	T+	114.34	113.633	0.707
CYS 64	7.60	7.643	0.043	C E+	111.72	111.488	0.232
ASN 65	8.27	8.155	-0.115	B E*	117.94	117.922	0.018
ASP 66	9.65	9.375	-0.275	T*	129.88	129.631	0.249
GLY 67	8.34	8.378	0.038	T*	108.70	108.854	-0.154
ARG 68				T	117.24		
THR 69	8.20	8.140	-0.060	T	119.5	119.613	-0.113
PRO 70				T*			
GLY 71	8.69	8.580	-0.110	T+	110.44	110.433	0.007

SER 72	7.30	7.350	0.050	T+	112.04	112.370	-0.330
ARG 73				C	124.20		
ASN 74	8.18	8.173	-0.007	T	115.28	115.745	-0.465
LEU 75	9.03	8.930	-0.100	T	118.4	118.415	-0.015
CYS 76	9.46	9.402	-0.058	T*	113.14	113.105	0.035
ASN 77	8.04	7.911	-0.129	T*	120.28	120.844	-0.564
ILE 78	8.79	8.622	-0.168	C E*	116.90	116.446	0.454
PRO 79				B E*			
CYS 80	8.24	8.266	0.026	G	123.08	123.091	-0.011
SER 81	8.58	8.471	-0.109	G*	112.96	112.754	0.206
ALA 82	7.61	7.604	-0.335	G*	125.10	124.919	0.181
LEU 83	7.85	7.931	0.081	G*	114.74	114.652	0.088
LEU 84	7.13	7.151	0.021	C T	118.04	118.485	-0.445
SER 85	6.83	6.902	0.072	T	112.94	113.141	-0.201
SER 86	8.50	8.538	0.038	T	118.36	118.593	-0.233
ASP 87	8.16	8.140	-0.020	T	120.12	120.422	-0.302
ILE 88	8.11	8.173	0.063	H	118.28	118.590	-0.310
THR 89	8.38	8.362	-0.018	H+	119.92	120.348	-0.428
ALA 90	9.11	8.917	-0.193	H+	121.86	122.001	-0.141
SER 91	7.79	7.893	0.103	H+	115.08	116.059	-0.979
VAL 92	8.38	8.307	-0.073	H+	120.60	120.489	0.111
ASN 93	8.66	8.591	-0.069	H	118.38	118.696	-0.316
CYS 94	7.91	7.926	0.016	H	117.34	117.254	0.086
ALA 95	8.70	8.640	-0.060	H	122.9	122.986	-0.086
LYS 96	8.01	7.997	-0.013	H*	114.98	114.899	0.081
LYS 97	7.23	7.299	-0.260	H*	120.98	121.333	-0.353
ILE 98	7.98	7.985	0.005	H*	121.12	121.227	-0.107
VAL 99	8.26	8.268	0.008	H	116.14	116.375	-0.235
SER 100	7.65	7.645	-0.005	H	115.38	114.617	0.763
ASP 101	8.03	7.993	-0.037	T C	119.98	120.176	-0.196
GLY 102	8.14	8.100	-0.040	T C	107.40	107.200	0.197
ASN 103				T*	117.94		
GLY 104	8.23	8.068	-0.162	G T*	107.60	107.300	0.316
MET 105	7.06	6.983	-0.077	G T*	119.22	119.083	0.137
ASN 106				G T+	114.68		
ALA 107	6.75	6.891	0.141	G T+	118.66	119.258	-0.598
TRP 108	7.88	7.839	-0.041	C T+	117.98	117.922	0.058
VAL 109	8.91	9.008	0.098	H G+	128.44		
ALA 110	8.00	7.823	-0.177	H G*	118.50	118.344	0.156
TRP 111	7.26	7.114	-0.146	H G*	114.70	114.688	0.012
ARG 112	8.23	8.133	-0.097	H T*	121.30	120.700	0.600
ASN 113	7.97	7.899	-0.071	H T*	112.64	112.683	-0.043

ARG 114	7.66	7.596	-0.064	H T	113.90	114.617	-0.717
CYS 115	7.35	7.399	0.049	H T	113.34	113.284	0.056
LYS 116	7.06	7.060	0	T	123.84	123.618	0.222
GLY 117	8.70	8.705	0.005	T	114.32	114.723	-0.403
THR 118	7.65	7.643	-0.007	T	109.92	110.152	-0.232
ASP 119	8.66	8.482	-0.178	T C	117.88	118.344	-0.464
VAL 120	8.13	8.140	0.010	G*	120.32	120.598	-0.278
GLN 121	8.46	8.396	-0.064	G	121.00	120.946	0.054
ALA 122	7.70	7.735	0.035	G	121.82	122.001	-0.181
TRP 123	7.61	7.588	-0.022	G T	114.20	114.617	-0.417
ILE 124	7.55	7.577	0.027	G T	108.60	108.921	-0.321
ARG 125	7.33	7.354	0.024	T	125.34	125.025	0.315
GLY 126	9.12	8.999	-0.121	T	113.54	113.598	-0.058
CYS 127	7.47	7.528	0.058	T*	116.16	116.375	-0.215
ARG 128	8.90	8.735	-0.165	C*	125.40	125.482	-0.082
LEU 129	7.96	7.795	-0.165	C*	129.94	130.686	-0.746

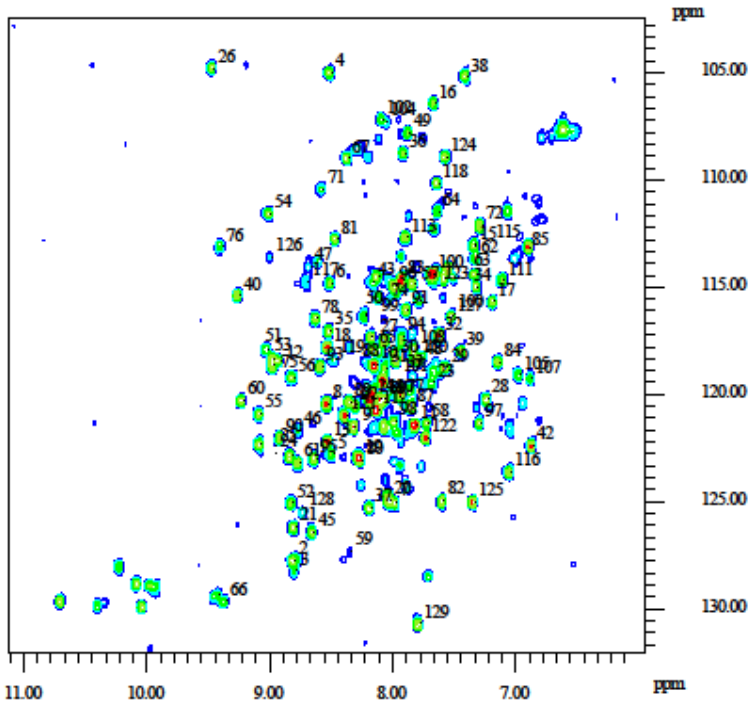

FIGURE S5: Natural abundance ^{15}N-^{1}H HSQC of 5mM HEWL pH 3.8, T = 70°C.

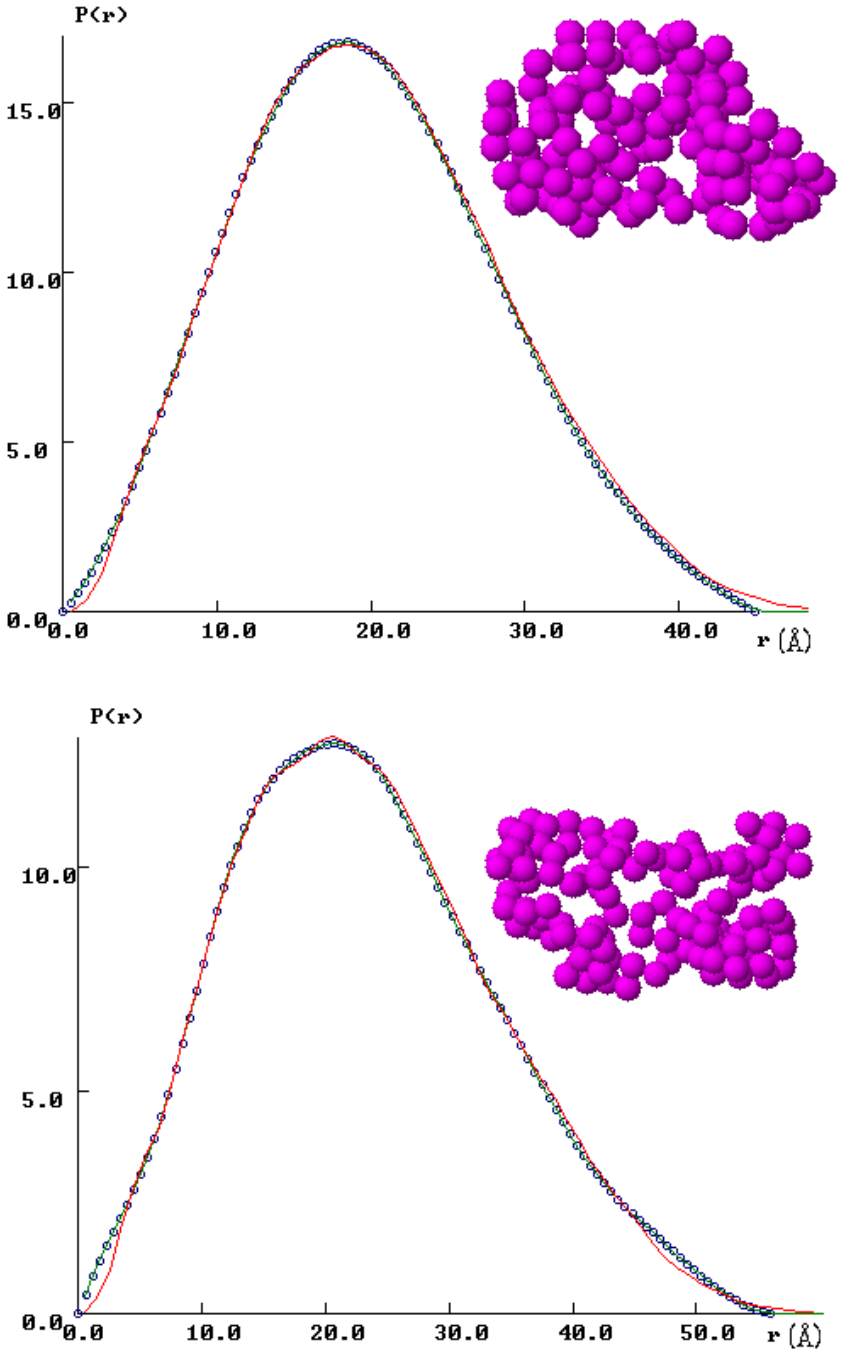

FIGURE S6: Distance distribution of HEWL at 20°C (top) and 80°C (bottom) calculated from the SAXS pattern. To minimize the effects of intermolecular interaction in concentrated solutions only data with $Q \geq 0.15$ Å were used for easier comparison with earlier work (36), using the program GNOM (22) to circumvent the limitation of the Q-range of Guinier's law ($QRg \leq 1.3$). The repulsive interactions may, however, influence the scattering pattern of HEWL even above $Q = 0.2$ Å^{-1} (37).

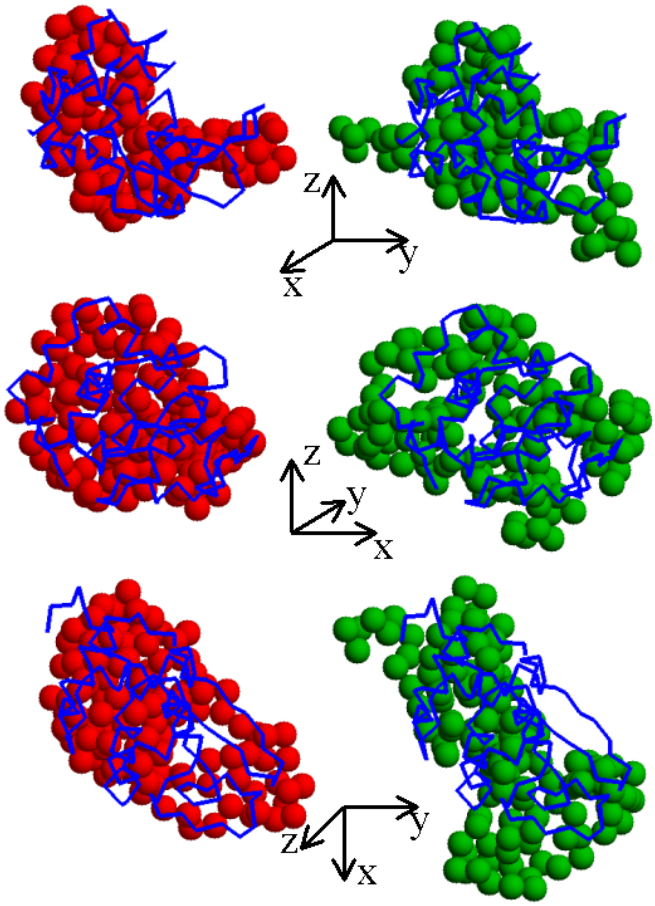

FiIGURE S7: Views in three orientations of SAXS models of HEWL obtained with the program GASBOR (23) (left: 20°C, right 80°C) superimposed to the trace of chain in PDB entry 6LYZ(1), illustrating the changes in the thermally unfolded protein.

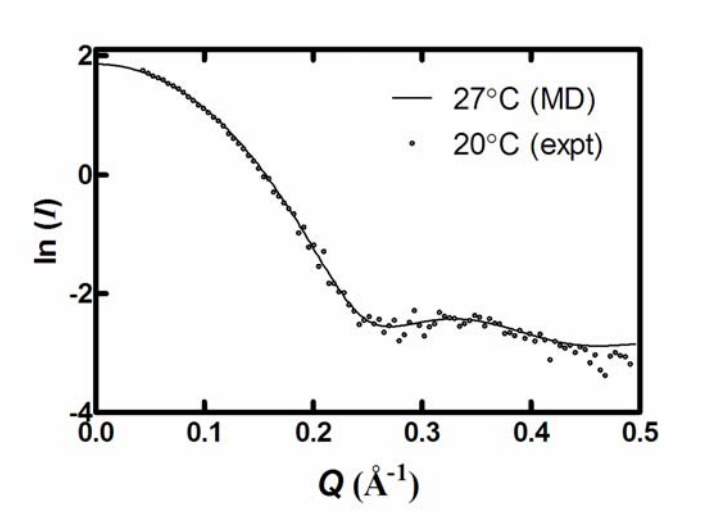

FIGURE S8: Comparison between experimental SAXS data for HEWL at 20°C and the initial MD structure obtained by equilibration for 2ns of 6LYZ at 27°C.

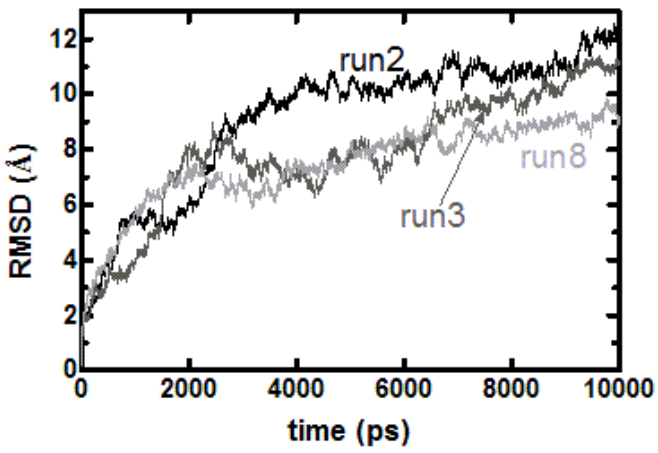

FIGURE S9: RMSD for three selected MD trajectories, starting from the initial structure in Fig. S1.

Time course of the secondary structure in the MD simulations

The secondary structure content calculated with the STRIDE algorithm (33) indicates that the sheet structures are completely lost after 1 ns for most trajectories and by 2 ns in the remaining ones. In contrast, most of the helix content is preserved at this time. Thus, the initial expansion of the structure evidenced by the increase in RMSD is due to the conversion of the β–structures to coil. This contradicts previous MD simulations with enhanced solvent penetration and some earlier work ((38) and references therein), where the β–structures remained intact throughout the unfolding process, but is in agreement with a later study where an unfolded β-domain and a structured α–domain were found (39, 40) and with the NMR results.

The helices, which start unfolding after the main increase in RMSD, behave differently in the various trajectories. Helix 1 [5-15] is mostly intact, but sometimes frays at its N-terminal end in agreement with the NMR results. Helix 3 [80-84], which is associated with large differences in amide proton chemical shifts (Δ^1H^N) remains also almost intact in all cases, but constantly expands and contracts between an α- and a 3_{10}-helix. Helix 5 [109-115], which has large Δ^1H^N at its two ends, is seldom completely lost, although it is unstable and occasionally loses its helicity only to regain it later. Its C-terminal end appears stable in NMR. Helices 2 [25-36] and 4 [88-101] are the least stable. In both cases, the central part is preserved throughout the trajectories, but either or both ends are found to fray during the course of the simulations. Unfolding of helices at their ends is also in agreement with the lower protection factor of these parts in amide hydrogen exchange experiments (35). In helix 4 [88-101] partial unfolding of either end is equally likely, in agreement with NMR. In helix 2 [25-36], this loss occurs more often at the C-terminal end, while in NMR the largest $^1H^N$ chemical shift differences are found at the N-terminal end. Comparison of crystal structures at different temperatures between -178°C and 22°C also indicates that all helices except helix 2 [25-36] are conserved with an RMSD better than 0.2 Å (41). A possible explanation for these apparently contradictory observations is that the helix is more mobile already at lower temperatures and that the differences at higher temperatures are therefore less pronounced.

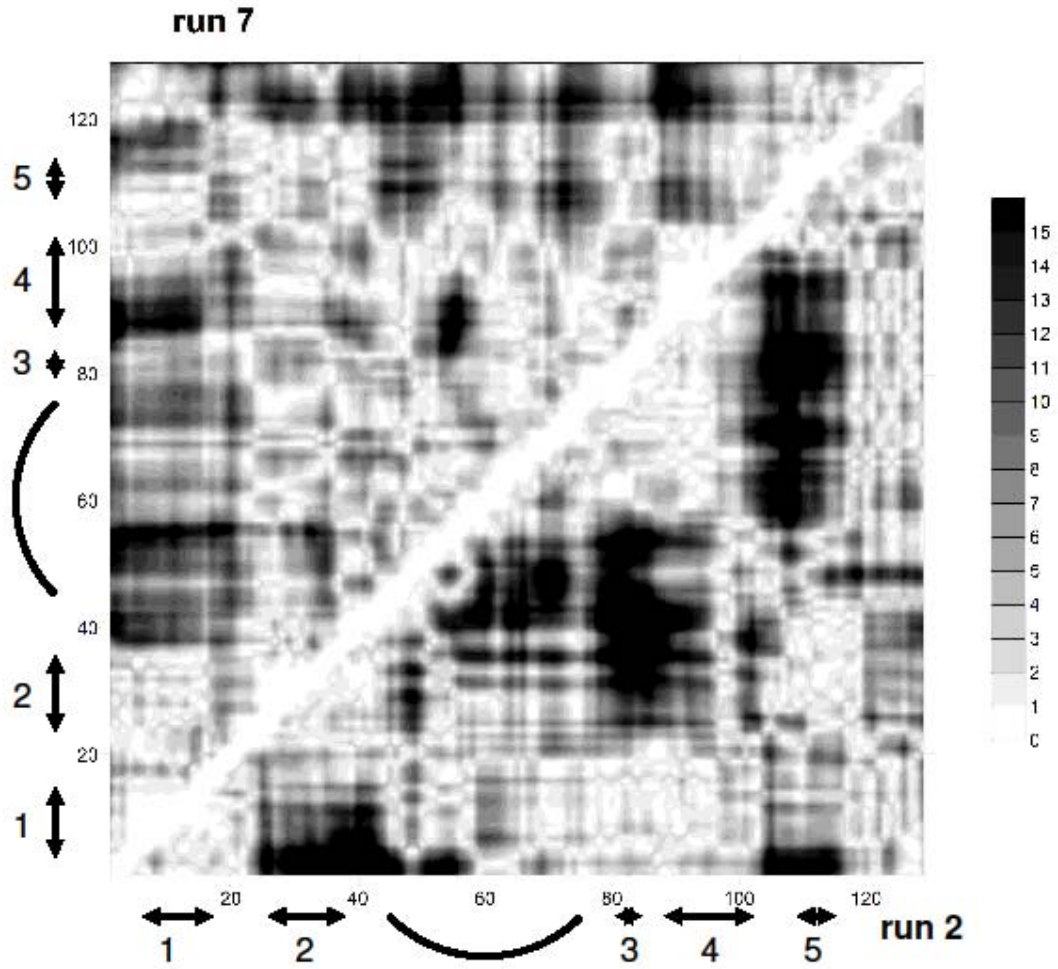

FIGURE S10: Absolute values of the differences between the distances between Cα-carbons in two MD models and the initial structure (*i.e.* $\left|d(C_\alpha(j),C_\alpha(i))_{\text{model}} - d(C_\alpha(j),C_\alpha(i))_{\text{initial}}\right|$). Top triangle, run 7, bottom triangle, run 2).

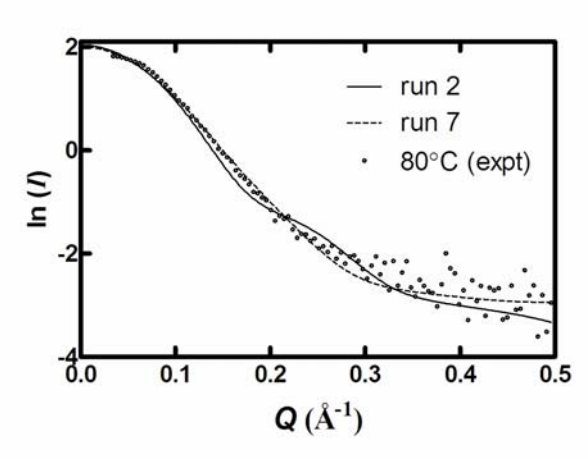

FIGURE S11: Comparison between the theoretical scattering patterns at the end of MD runs 2 and 7 and the experimental SAXS data at 80°C.

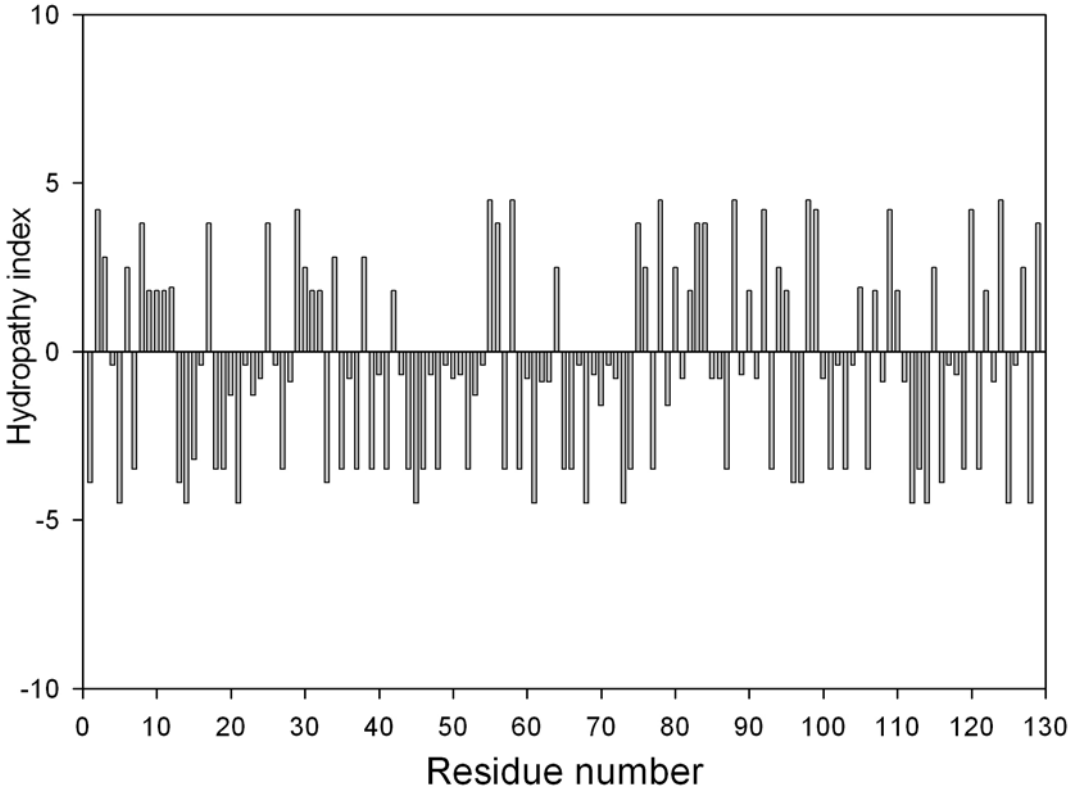

FIGURE S12: variation of the hydropathy index (42) of residues along the HEWL chain.

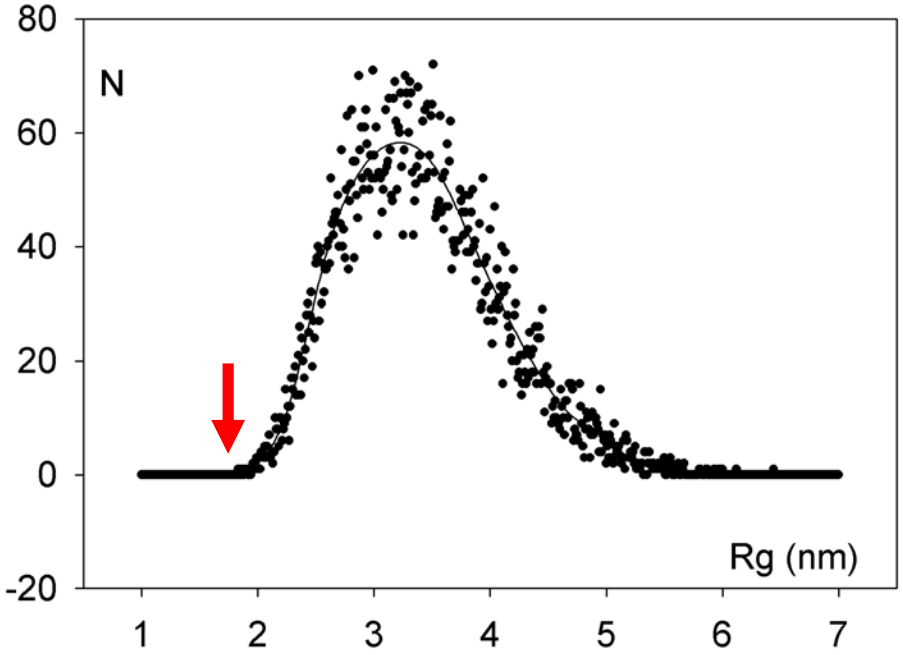

FIGURE S13: Rg-distribution for an excluded volume chain with 129 residues represented by spheres of 0.38 nm diameter (average distance between Cα atoms). The arrow indicates the maximum value observed for HEWL with intact disulphide bridges.

References

1. Diamond, R. 1974. Real-space refinement of the structure of hen egg-white lysozyme J. Mol. Biol. 82:371-391.
2. Miles, A. J., and B.A. Wallace. 2006. Synchrotron radiation circular dichroism spectroscopy of proteins and applications in structural and functional genomics. Chem. Soc. Reviews 35:39-51.
3. Lees, J. G., B.R. Smith, F. Wien, A.J. Miles, and B.A. Wallace. 2004. CDtool - An integrated software package for circular dichroism spectroscopic data processing, analysis and archiving. Anal. Biochem. 332:285-289.
4. Provencher, S. W., and J. Glockner. 1981. Estimation of globular protein secondary structure from circular dichroism. Biochemistry 20:33-37.
5. Van Stokkum, I. H. M., H.J.W. Spoelder, M. Bloemendal, R. Van Grondelle, and F.C.A. Groen. 1990. Estimation of protein secondary structure and error analysis from CD spectra. Anal. Biochem. 191:110-118.
6. Manavalan P., and W. C. Johnson, Jr. 1987. Variable selection method improves the prediction of protein secondary structure from circular dichroism spectra. Anal. Biochem. 167:76-85.
7. Sreerama, N., and R.W. Woody. 2000. Estimation of protein secondary structure from CD spectra: Comparison of CONTIN, SELCON and CDSSTR methods with an expanded reference set. Anal. Biochem. 287:252-260.
8. Whitmore, L., and B.A. Wallace. 2004. DICHROWEB, an online server for protein secondary structure analyses from circular dichroism spectroscopic data. Nucleic Acids Res. 32:W668-W673.
9. Whitmore, L., and B.A. Wallace. 2008. Protein secondary structure analyses from circular dichroism spectroscopy: Methods and reference databases. Biopolymers 89:392-400.
10. Sreerama, N., and R.W. Woody. 1993. A self-consistent method for the analysis of protein secondary structure from circular dichroism. Anal Biochem. 209:32-44.
11. Lees, J.G., A.J. Miles, R.W. Janes, B.A. Wallace. 2006. Optimisation and development of novel methodologies for secondary structure prediction from circular dichroism spectra. BMC Bioinformatics 7:507-517.
12. Lees, J. G., A.J. Miles, F. Wien, and B.A. Wallace. 2006. A reference database for circular dichroism spectroscopy covering fold and secondary structure space. Bioinformatics 22:1955-1962.
13. Mao, D., E. Wachter, and B.A. Wallace. 1982. Folding of the H^+-ATPase proteolipid in phospholipid vesicles. Biochemistry 21:4960-4968.
14. Smeller, L., K. Goossens, and K. Heremans. 1995. How to avoid artifacts in Fourier self-deconvolution. Appl. Spectrosc. 49:1538-1542.
15. Wishart, D. S., C.G. Bigam, J. Yao, F. Abildgaard, H.J. Dyson, E. Oldfield, J.L. Markley, and B.D. Sykes. 1995. ^{1}H, ^{13}C and ^{15}N chemical shift referencing in biomolecular NMR. J. Biomol. NMR 6:135-140.
16. Liu, M., X. Maoa, C. Yea, H. Huanga, J.K. Nicholson, and J.C. Lindon. 1998. Improved WATERGATE Pulse Sequences for Solvent Suppression in NMR Spectroscopy J. Magn. Reson. 132:125-129.
17. Gronwald, W., and H.R. Kalbitzer. 2004. Automated structure determination of proteins by NMR spectroscopy. Prog. NMR Spectr. 44:33-96.
18. Koch, M. H. J., and J. Bordas. 1983. X-ray diffraction and scattering on disordered systems using synchrotron radiation. Nucl. Instrum. and Methods 208:461-469.

19. Shang, W., B. Robrahn, F. Golding, and M.H.J. Koch. 2004. A versatile data acquisition system for time resolved X-ray scattering using gas proportional detectors with delay line readout. . Nuclear Instrum. and Methods A 530:513-520.
20. Gabriel, A. 1977. Position sensitive x-ray detector. Rev. Sci. Instrum. 48:1303-1305.
21. Boulin, C., R. Kempf, M.H.J. Koch, and S.M. Mc Laughlin. 1986. Data appraisal, evaluation and display for synchrotron radiation experiments: hardware and software. Nucl. Instruments and Methods A249:399-407.
22. Svergun, D. I. 1992. Determination of the regularization parameter in indirect-transform methods using perceptual criteria. J. Appl. Crystallogr. 25:495-503.
23. Svergun, D. I., M.V. Petoukhov, and M.H.J. Koch. 2001. Determination of domain structure of proteins from X-ray solution scattering. Biophys. J. 80:2946-2953.
24. Phillips, J. C., R. Braun, W. Wang, J. Gumbart, E. Tajkhorshid, E. Villa, C. Chipot, R. D. Skeel, L. Kale, and K. Schulten. 2005. Scalable Molecular Dynamics with NAMD. J. Comput. Chem. 26:1781-1802.
25. Berman, H. M., J. Westbrook, Z. Feng, G. Gilliland, T. N. Bhat, H. Weissig, I. N. Shindyalov and P. E. Bourne. 2000. The Protein Data Bank. Nucleic Acids Res. 28:235-242.
26. Humphrey, W., A. Dalke, and K. Schulten. 1996. VMD - Visual Molecular Dynamics. J. Mol. Graph. 14:33-38.
27. Brooks, B. R., R. E. Bruccoleri, B. D. Olafson, D. J. States, S. Swaminathan, and M. Karplus. 1983. Charmm: A Program for Macromolecular Energy, Minimization, and Dynamics Calculations. J. Comput. Chem. 4:187-217.
28. Darden, T., L. Perera, L. Li, and L. Pedersen. 1999. New Tricks for Modelers from the Crystallography Toolkit: The Particle Mesh Ewald Algorithm and Its Use in Nucleic Acid Simulations. Structure 7:R55-R60.
29. Anderson, H. C. 1983. Rattle: A 'Velocity' Version of the Shake Algorithm for Molecular Dynamics Calculations. J. Comput. Phys. 54:24-34.
30. Swope, W. C., H. C. Andersen, P. H. Berens and K. R. Wilson. 1982. A Computer Simulation Method for the Calculation of Equilibrium Constants for the Formation of Physical Clusters of Molecules: Application to Small Water Clusters. J. Chem. Phys. 76:637-649.
31. Redfield C, and C.M. Dobson 1988. Sequential 1H NMR assignments and secondary structure of hen egg white lysozyme in solution. Biochemistry 27:122-136.
32. Vaney, M. C., S. Maignan, M. Ries-Kautt, and A. Ducruix. 1996. High-resolution structure (1.33Å) of a HEW lysozyme tetragonal crystal grown in the APCF apparatus. Data and structural comparison with a crystal grown under microgravity from SpaceHab-01 mission. Acta Crystallogr. D 52:505-517.
33. Frishman, D., and P. Argos. 1995. Knowledge-Based Protein Secondary Structure Assignment. . Proteins-Structure Function and Genetics 23:566-579.
34. Schwalbe, H., S.B. Grimshaw, A. Spencer, M. Buck, J. Boyd, C.M. Dobson, C. Redfield and L.J. Smith. 2001. A refined solution structure of hen lysozyme determined using residual dipolar coupling data. Protein Sci. 10:677-688.
35. Radford, S. E., M. Buck, K.D. Topping, C.M. Dobson, and P.A. Evans. 1992. Hydrogen exchange in native and denatured states of hen egg-white lysozyme. Proteins: Structure, Function, and Genetics 14:237-248.
36. Arai, S., and M. Hirai. 1999. Reversibility and hierarchy of thermal transition of hen egg-white lysozyme studied by small angle X-ray scattering. Biophys. J. 76:2192-2197.
37. Niebuhr, M., and M.H.J. Koch. 2005. Effects of urea and trimethylamine-N-oxide (TMAO) on the interactions of lysozyme in solution. A small angle X-ray scattering study. Biophys. J. 89:1978-1984.

38. Williams, M. A., J.M. Thornton, and J.M. Goodfellow. 1997. Modelling protein unfolding: hen egg-white lysozyme. Protein Engineering 10:895-903.
39. Kazmirski, S. L., and V. Daggett. 1998. Non-native interactions in protein folding intermediates: molecular dynamics simulations of hen lysozyme. J. Mol Biol. 284:793-806.
40. Gilquin, B., C. Guilbert, and D. Perahia. 2000. Unfolding of Hen Egg Lysozyme by Molecular Dynamics simulations at 300K: insight into the role of the interdomain interface. . Proteins: Structure, Function, and Genetics 41:58-74.
41. Kurinov, I. V., and R.W. Harrison. 1995. The influence of temperature on lysozyme crystals. Structure and dynamics of protein and water. Acta Crystallogr D Biol Crystallogr. 51:98-109.
42. Kyte, J., and R.F. Doolittle. 1982. A simple method for displaying the hydropathic character of a protein. J. Mol. Biol. 157:105-132.